https://doi.org/10.31436/iiumej.v25i2.3119

ATTITUDE UAV STABILITY CONTROL USING LINEAR QUADRATIC REGULATOR-NEURAL NETWORK (LQR-NN)

OKTAF AGNI DHEWA[1], FATCHUL ARIFIN[2*], ARDY SETO PRIAMBODO[1], ANGGUN WINURSITO[2], YASIR MOHD. MUSTAFAH[3]

[1]Dept. of Electrical and Electronic Engineering, Vocational Faculty, Universitas Negeri Yogyakarta, Yogyakarta, Indonesia
[2]Dept. of Electronics and Informatics Engineering, Faculty of Engineering, Universitas Negeri Yogyakarta, Yogyakarta, Indonesia
[3]Dept. of Mechatronics Engineering, Kulliyyah of Engineering, International Islamic University Malaysia, Selangor, Malaysia

**Corresponding author: fatchul@uny.ac.id*

(Received: 20 November 2023; Accepted: 11 May 2024; Published online: 15 July 2024)

ABSTRACT: The stability of an Unmanned Aerial Vehicle (UAV) attitude is crucial in aviation to mitigate the risk of accidents and ensure mission success. This study aims to optimize and adaptively control the flight attitude stability of a flying wing-type UAV amidst environmental variations. This is achieved through the utilization of Linear Quadratic Regulator-Neural Network (LQR-NN) control, wherein the Neural Network predicts the optimal K gain value by fine-tuning Q and R parameters to minimize system errors. An online learning neural network adjusts the K value based on real-time error feedback, enhancing system performance. Experimental results demonstrate improved stability metrics: for roll angle stability, a rise time of 0.4682 seconds, settling time of 1.3819 seconds, overshoot of 0.298%, and Steady State Error (SSE) of 0.133 degrees; for pitch angle stability, a rise time of 0.2309 seconds, settling time of 0.7091 seconds, overshoot of 0.1224%, and Steady State Error (SSE) of 0.0239 degrees. The LQR-NN approach effectively reduces overshoot compared to traditional Linear Quadratic Regulator (LQR) control, thereby minimizing oscillations. Furthermore, LQR-NN can minimize the Steady State Error (SSE) to 0.074 degrees for roll rotation motion and 0.035 degrees for pitch rotation motion.

ABSTRAK: Kestabilan perubahan Pesawat Tanpa Pemandu (UAV) adalah penting dalam penerbangan bagi mengurangkan risiko kemalangan dan memastikan kejayaan misi. Kajian ini bertujuan mengoptimum dan menstabilkan perubahan kawalan adaptif penerbangan UAV jenis sayap terbang di tengah-tengah variasi persekitaran. Ini dicapai melalui penggunaan kawalan Rangkaian Linear Kuadratik Pengatur-Neural (LQR-NN), di mana Rangkaian Neural meramal nilai perolehan K optimum dengan meneliti parameter Q dan R bagi mengurangkan ralat sistem. Rangkaian neural pembelajaran dalam talian melaraskan nilai K berdasarkan maklum balas ralat masa nyata, ini meningkatkan prestasi sistem. Dapatan kajian eksperimen menunjukkan metrik kestabilan lebih baik: bagi kestabilan sudut gulungan, masa kenaikan sebanyak 0.4682 saat, masa kestabilan 1.3819 saat, lajakan 0.298% dan Ralat Keadaan Mantap (SSE) 0.133 darjah; bagi kestabilan sudut pic, masa kenaikan 0.2309 saat, masa penetapan 0.7091 saat, lajakan 0.1224%, dan Ralat Keadaan Mantap (SSE) 0.0239 darjah. Pendekatan LQR-NN berkesan mengurangkan lajakan berbanding kawalan tradisi Pengatur Kuadratik Linear (LQR), dengan itu mengurangkan ayunan. Tambahan, LQR-NN dapat mengurangkan Ralat Keadaan Mantap (SSE), sebanyak 0.074 darjah bagi gerakan putaran guling dan 0.035 darjah bagi gerakan putaran anggul.

KEYWORDS: *Unmanned Aerial Vehicle, Optimal Control, Adaptive, Linear Quadratic Regulator, Neural Network*

https://doi.org/10.31436/iiumej.v25i2.3119

1. INTRODUCTION

Unmanned Aerial Vehicles (UAVs), more commonly known as drones, have become a very important and transformational technology in various aspects of human life and the industrial sector [1]. The current use of UAVs has various positive implications that reflect significant impacts in various fields, such as monitoring and surveillance, photography, delivery of goods, precision agriculture, infrastructure monitoring, security, and so on [2].

One type of UAV that is the focus of development in carrying out this task is the flying wing [3]. A flying wing is an aircraft design that does not have a conventional fuselage or tail and consists almost entirely of wings [4]. This type of UAV has superior aerodynamic efficiency, which provides the ability to fly longer distances compared to other designs [5]. In addition, they have good maneuverability, resistance to different environmental conditions, and the ability to carry various types of sensor payloads and cargo [6].

Of course, in carrying out these sector missions, the flying wing UAV is supported by an autonomous system that requires good stability control [7]. Stability control is the main factor in the success of an aircraft flight. Without good stability, an aircraft cannot maintain the correct height, direction, attitude, and position, making it difficult to operate or even risk an accident [8].

One of the effective control systems for maintaining UAV flight stability is the Linear Quadratic Regulator (LQR). Recent research indicates that employing LQR control in managing UAV attitude enables swift error correction, ensuring the maintenance of desired steady-state values [9,10]. Utilizing LQR control allows the UAV to minimize system errors with stability responses across all three orientation angles (roll, pitch, and yaw) in less than 1 second [11]. Fundamentally, LQR is a control method grounded in optimal control theory [12], utilized to design optimal controllers for linear systems, particularly within the context of dynamic systems represented by linear differential equations. LQR aims to generate control signals that minimize specified performance criteria [13]. Nonetheless, LQR encounters challenges in adapting to dynamic environmental changes, necessitating the development or incorporation of methods to optimize aircraft stability in constantly evolving scenarios [14].

Hence, there is a demand for a control system that exhibits robust characteristics and adapts to handle the intricacies of tasks and prevailing environmental conditions. The adaptability of LQR can be enhanced by integrating a Neural Network, enabling the adjustment of LQR feedback gain values to suit prevailing conditions, thereby optimizing its performance in that environment [15]. Implementing the LQR control system with a Neural Network on a quadcopter-type UAV has yielded fairly satisfactory outcomes. Neural networks have significantly enhanced the aircraft's response to rotational and translational motion, nearing the desired specifications [16]. Building upon this, this research focuses on LQR with Neural Network integration, referred to as LQR-NN. LQR-NN will be applied to a flying wing-type UAV model. Given the heightened susceptibility to dynamic changes in flying wing-type UAV flights, precise accommodation, and high performance are anticipated to mitigate errors.

2. UAV FLYING WING MODELING

Designing a control system requires kinematics and dynamic modeling of the aircraft. Modeling begins by examining the forces acting on the UAV flying wing aircraft [17]. The forces are visualized in aircraft body motion, as in Figure 1 [18].

https://doi.org/10.31436/iiumej.v25i2.3119

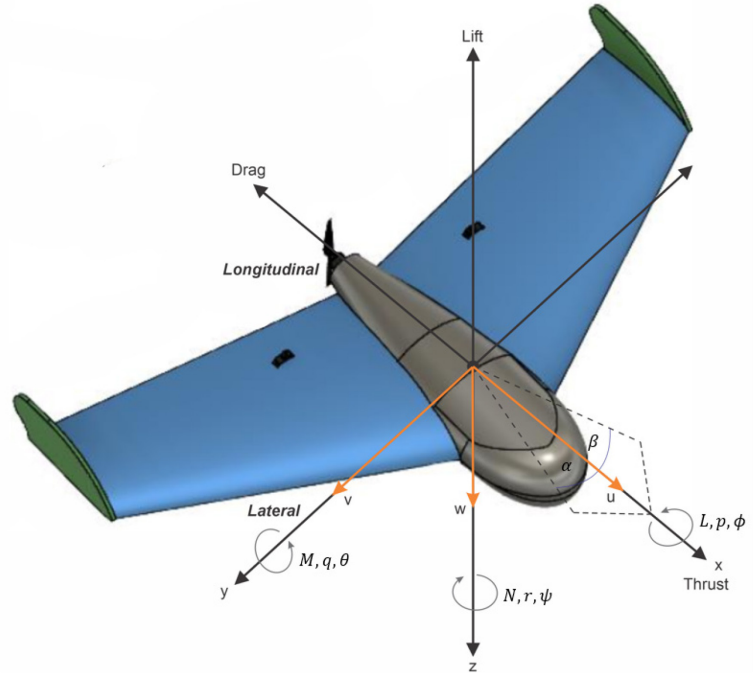

Figure 1. Flying wing UAV motion axis

During flight, an airplane can rotate along three axes (x, y, and z) concerning its center of mass. The aircraft's position control system typically manages its angular orientation by adjusting angles. Various aerodynamic forces come into play when an object is airborne, including lift, thrust, weight, and drag. These forces are crucial in determining the aircraft's behavior and maneuverability in the air.

Aircraft do not consistently maintain a strictly horizontal path while advancing [19]. This phenomenon arises from either air deflection from the front along the x-axis or from the side along the y-axis. Air deflection from the front results in the angle of attack ($\alpha - alpha$), whereas deflection from the side leads to the aircraft's sideslip angle ($\beta - beta$). The equations for these two angles deflection are as follows:

$$\alpha = tan^{-1}\frac{w}{u} \tag{1}$$

$$\beta = tan^{-1}\left(\frac{v}{\sqrt{u^2+w^2}}\right) \tag{2}$$

The system uses the North East Down (NED) frame for the Earth and aircraft body frame. So, the body frame and the NED frame can be related using a rotation matrix. The formula of a rotation matrix is defined in Eq. (1).

$$\begin{bmatrix} cos\psi cos\theta & -sin\psi cos\phi + cos\psi sin\theta sin\phi & sin\psi sin\phi + cos\psi cos\phi sin\theta \\ sin\psi cos\theta & cos\psi cos\phi + sin\phi sin\theta sin\psi & -cos\psi sin\phi + sin\theta sin\psi cos\phi \\ -sin\theta & cos\theta sin\phi & cos\theta cos\phi \end{bmatrix} \tag{3}$$

The correlation between frames generates rotational angles utilized for aircraft orientation. The rotation angles employed in the system are known as Euler angles. The Euler angles use

https://doi.org/10.31436/iiumej.v25i2.3119

roll (ϕ), pitch (θ), and yaw (ψ) angles. Each orientation angle has a derivative of angular velocity as a form of controlled state.

$$\begin{bmatrix} p \\ q \\ r \end{bmatrix} = \begin{bmatrix} 1 & 0 & -sin\theta \\ 0 & cos\phi & cos\theta sin\phi \\ 0 & -sin\phi & cos\theta cos\phi \end{bmatrix} \begin{bmatrix} \dot{\phi} \\ \dot{\theta} \\ \dot{\psi} \end{bmatrix} \tag{4}$$

p is the roll rate or the angular velocity of the y-axis, q is the pitch rate or the angular velocity of the x-axis, and p is the yaw rate or the angular velocity of the z-axis. Where,

$$\dot{\phi} = \frac{d\phi}{dt} \tag{5}$$

$$\dot{\theta} = \frac{d\theta}{dt} \tag{6}$$

$$\dot{\psi} = \frac{d\psi}{dt} \tag{7}$$

Furthermore, the aircraft's translation velocity along each axis (x, y, and z) is interconnected. The translation velocity along each axis is dictated by alterations in the plane frame's translation relative to the ground frame.

$$\begin{bmatrix} \dot{x} \\ \dot{y} \\ \dot{z} \end{bmatrix} = \begin{bmatrix} cos\psi cos\theta & -sin\psi cos\phi + cos\psi sin\theta sin\phi & sin\psi sin\phi + cos\psi cos\phi sin\theta \\ sin\psi cos\theta & cos\psi cos\phi + sin\phi sin\theta sin\psi & -cos\psi sin\phi + sin\theta sin\psi cos\phi \\ -sin\theta & cos\theta sin\phi & cos\theta cos\phi \end{bmatrix} \begin{bmatrix} u \\ v \\ w \end{bmatrix} \tag{8}$$

where u is the translational velocity of the x-axis, v is the translational velocity of the y-axis, w is the translational velocity of the z-axis.

Both kinematic and dynamic models can characterize the aircraft system. These models were employed to formulate equations for the forces, moments, and orientation angles present within the system, which are visualized in the aircraft's two motions. The aircraft's motion is classified into translational and rotational components [20].

The determination of an aircraft's translational movement is carried out using the Newton-Euler law, which is based on Newton's second law.

$$\sum F = m.a \tag{9}$$

where m is mass (kg), and a is acceleration ($\frac{m}{s^2}$).

$$\sum F = F + F_{gravity} \tag{10}$$

$$\sum F = m\frac{d}{dt}v_T = m\frac{d}{dt}v_T + (\omega x v_T) \tag{11}$$

where v_T is the translational velocity ($\frac{m}{s}$) and ω is angular velocity.

The linear and total angular vector velocities can be calculated with Eq. (12) and (13),

$$v_T = iu + jv + kw \tag{12}$$

$$\omega = ip + jq + kr \tag{13}$$

where i, j, k are vector directions. The derivate of the linear velocity can be calculated with Eq. (14).

https://doi.org/10.31436/iiumej.v25i2.3119

$$\frac{d}{dt}v_T = i\dot{u} + j\dot{v} + k\dot{w} \tag{14}$$

Thus, the states that occur on the plane can be written in the following matrix [21],

$$\omega x v_T = \begin{bmatrix} i & j & k \\ p & q & r \\ u & v & w \end{bmatrix} = (qw - vr) + (ur - pw) + (pv - uq) \tag{15}$$

By involving linear and angular velocity, the total forces acting on the system can be expressed,

$$\sum F = \{i\dot{u} + j\dot{v} + k\dot{w} + ((qw - vr) + (ur - pw) + (pv - uq))\} \tag{16}$$

$$\sum F = \{i(\dot{u} + qw - vr) + j(\dot{v} + ur - pw) + k(\dot{w} + pv - uq)\} \tag{17}$$

$$\sum F = \{i\sum F_x + j\sum F_y + k\sum F_z\} \tag{18}$$

So, based on Eq. (17) and (18), the forces of each axis can be calculated with this formula,

$$\sum F_x = \dot{u} + qw - vr \tag{19}$$

$$\sum F_y = \dot{v} + ur - pw \tag{20}$$

$$\sum F_z = \dot{w} + pv - uq \tag{21}$$

Every axis of the plane is affected by the force of gravity. Thus, Eq. (19) to (21) will transform into Eq. (22) to (24), where g is the gravitational acceleration.

$$\frac{F_x - mg.sin\theta}{m} = \dot{u} + qw - vr \tag{22}$$

$$\frac{F_y + mg.cos\theta sin\phi}{m} = \dot{v} + ur - pw \tag{23}$$

$$\frac{F_z + mg.cos\theta cos\phi}{m} = \dot{w} + pv - uq \tag{24}$$

Because $F_x = X$, $F_y = Y$, and $F_z = Z$, the forces equation on each plane axis can be written as,

$$\frac{X}{m} - g.sin\theta = \dot{u} + qw - vr \tag{25}$$

$$\frac{Y}{m} + g.cos\theta sin\phi = \dot{v} + ur - pw \tag{26}$$

$$\frac{Z}{m} + g.cos\theta cos\phi = \dot{w} + pv - uq \tag{27}$$

Furthermore, the rotational motion of an aircraft is defined through the angular momentum acting on the system. The momentum has the following equation,

$$H = I\omega \tag{28}$$

where H is angle momentum ($\frac{\text{kg.m}^2\text{.rad}}{\text{s}}$) and I is inertia moment (kg.m^2). Eq (29) can describe the inertia moment,

$$I = \begin{bmatrix} I_{xx} & -I_{xy} & -I_{xz} \\ -I_{xy} & I_{yy} & -I_{yz} \\ -I_{xz} & -I_{yz} & I_{zz} \end{bmatrix} \tag{29}$$

The torque that occurs in the system is

$$M = I\frac{d}{dt}(\omega + \omega x\omega) + \omega xH \tag{30}$$

when $\omega x\omega = 0$, then Eq. (30) can be rewritten as in Eq. (31) and (32) [22].

https://doi.org/10.31436/iiumej.v25i2.3119

$$\frac{d}{dt}\omega = ip + jq + kr \tag{31}$$

$$\omega xH = \begin{vmatrix} i & j & k \\ p & q & r \\ h_x & h_y & h_z \end{vmatrix} \tag{32}$$

The evaluation of the determinant with unit vectors i, j, and k, along with angular momentum projections, can be expressed as a cross-product calculation in Eq. (33).

$$\omega xH = \left(qh_z - rh_y\right)i + (rh_x - ph_z)j + \left(ph_y - qh_x\right)k \tag{33}$$

The moment of inertia that occurs on the three axes of the aircraft is described in Eq. (32), with h_x, h_y, and h_z are defined in Eq. (35).

$$H = I\omega = \begin{bmatrix} I_{xx} & -I_{xy} & -I_{xz} \\ -I_{xy} & I_{yy} & -I_{yz} \\ -I_{xz} & -I_{yz} & I_{zz} \end{bmatrix} \begin{bmatrix} p \\ q \\ r \end{bmatrix} \tag{34}$$

$$\begin{bmatrix} h_x \\ h_y \\ h_z \end{bmatrix} = \begin{bmatrix} I_{xx}p - I_{xy}q - I_{xz}r \\ -I_{xy}p + I_{yy}q - I_{yz}r \\ -I_{xz}p - I_{yz}q + I_{zz}r \end{bmatrix} \tag{35}$$

The aircraft has a symmetrical shape about the XZ axis, so $I_{xy} = I_{yz} = 0$. So, Eq. (34) transform to Eq. (36).

$$\begin{bmatrix} h_x \\ h_y \\ h_z \end{bmatrix} = \begin{bmatrix} I_{xx}p - I_{xz}r \\ I_{yy}q \\ -I_{xz}p + I_{zz}r \end{bmatrix} \tag{36}$$

Substituting Eq. (36) into Eq. (33) yields:

$$\omega xH = \left(q(-I_{xz}p + I_{zz}r) - r(I_{yy}q)\right)i + \left(r(I_{xx}p - I_{xy}q) - p(-I_{xz}p + I_{zz}r)\right)j + \left(p(I_{yy}q) - q(I_{xx}p - I_{xy}q)\right)k \tag{37}$$

$$\omega xH = \left(-I_{xz}pq + I_{zz}qr) - I_{yy}qr\right)i + (I_{xx}pr - I_{xz}r^2 + I_{xz}p^2 - I_{zz}pr)j + \left(I_{yy}pq - I_{xx}pq + I_{xz}qr\right)k \tag{38}$$

The derivate of angle momentum can be calculated,

$$I\frac{d}{dt}\omega = \begin{bmatrix} I_{xx}\dot{p} - I_{xz}\dot{r} \\ I_{yy}\dot{q} \\ -I_{xz}\dot{p} + I_{zz}\dot{r} \end{bmatrix} \tag{39}$$

According to Eq. (30), the torque in each axis rotation can be expressed by adding Eq.(38) and (39)[23],

$$M_x = L = I_{xx}\dot{p} - I_{xz}(\dot{r} + pq) + (I_{zz} - I_{yy})qr \tag{40}$$

$$M_y = M = I_{yy}\dot{q} - I_{xz}(p^2 + q^2) + (I_{xx} - I_{zz})pr \tag{41}$$

$$M_z = N = I_{zz}\dot{r} - I_{xz}\dot{p} + \left(I_{xx} - I_{yy}\right)pq + I_{xz}qr \tag{42}$$

This study's stability observations were conducted solely on rotational motions around the x and y axes. Consequently, the force affecting motion along the z-axis can be disregarded. Therefore, the torque equations in Eq. (40) to (42) can be simplified to:

$$M_x = L = I_{xx}\dot{p} + (I_{zz} - I_{yy})qr \tag{43}$$

$$M_y = M = I_{yy}\dot{q} + (I_{xx} - I_{zz})pr \tag{44}$$

Eq. (43) represents the rotational movement of the aircraft about the x-axis, incorporating x-axis inertia (I_{xx}), roll angular acceleration ($\dot{p}$), pitch rate (q), and yaw rate (r). This can be expressed as a transfer function in Eq. (45).

$$\dot{p} = \frac{L}{I_{xx}} - \frac{(I_{zz} - I_{yy})qr}{I_{xx}} \tag{45}$$

Similarly, in Eq. (44), which depicts the rotational motion of the aircraft around the y-axis, incorporating y-axis inertia (I_{yy}), pitch angular acceleration ($\dot{q}$), roll rate (p), and yaw rate (r). This can be formulated into a transfer function in Eq. (46).

$$\dot{q} = \frac{M}{I_{yy}} - \frac{(I_{xx} - I_{zz})pr}{I_{yy}} \tag{46}$$

3. LQR-NN Control Design

A linear quadratic regulator is a control method that is called linear because the controller's model and shape are linear. It is also called quadratic because the cost function is quadratic. Meanwhile, it is called a Regulator because the reference is not a function of time. Figure 2 depicts the block diagram of the LQR control system.

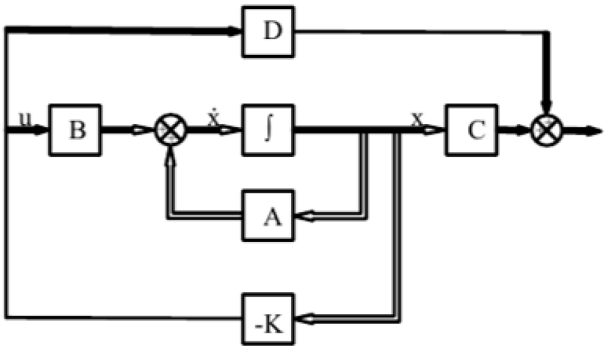

Figure 2. Full state feedback LQR

The LQR control system works on a linear system with calculations shown in Eq. (47) to (50).

$$\dot{\boldsymbol{x}} = \boldsymbol{Ax} + \boldsymbol{Bu} \tag{47}$$

$$\boldsymbol{y} = \boldsymbol{Cx} + \boldsymbol{Du} \tag{48}$$

$$\boldsymbol{u} = -\boldsymbol{Kx} \tag{49}$$

$$\dot{\boldsymbol{x}} = (\boldsymbol{A} - \boldsymbol{BK})\boldsymbol{u} \tag{50}$$

In designing the control system to be optimal, energy minimization (cost function/quadratic function) is carried out, which is defined through the performance index in the interval [t0, ∞] in Eq. (51)[24]. This function involves Q and R matrices to make the system matrix non-negative.

$$\boldsymbol{J} = \int_{t_0}^{\infty} (\boldsymbol{x}^T \boldsymbol{Qx} + \boldsymbol{u}^T \boldsymbol{Ru}) dt \tag{51}$$

K determines the index performance to reach the minimum value. Finding the optimal value of K requires solving a quadratic regulator using the Riccati equation. The Riccati equation is a first-order form of a differential equation, which is an unknown quadratic function. This solution adds a differential equation with a constant P matrix [25]. This equation is shown in Eq. (52).

https://doi.org/10.31436/iiumej.v25i2.3119

$$\boldsymbol{J} = \int_{t_0}^{\infty} \frac{d}{dt}(\boldsymbol{x}^T \boldsymbol{P}\boldsymbol{x})\, dt = \boldsymbol{x}^T(0)\boldsymbol{P}\boldsymbol{x}(0) \tag{52}$$

From the reduction carried out by the Riccati equation, the determination of the K value is finalized using the Hamilton – Jacobian – Bellman procedure, which is calculated via Eq. (53) and produces Eq. (54) as the final solution.

$$\boldsymbol{K} = \boldsymbol{R}^{-1}\boldsymbol{B}^T\boldsymbol{P} \tag{53}$$

$$\boldsymbol{A}^T\boldsymbol{P} + \boldsymbol{P}\boldsymbol{A} + \boldsymbol{Q} - \boldsymbol{P}\boldsymbol{B}\boldsymbol{R}^{-1}\boldsymbol{B}^T\boldsymbol{P} \tag{54}$$

Based on the explanation of the equations and characteristics of the LQR control system, it requires a system model in the form of a linear approach. Therefore, referring to the model equation in the previous subsection, the linearization equation of the aircraft model can be written as follows [26],

$$\begin{bmatrix} U \\ \dot{U} \\ V \\ \dot{V} \\ W \\ \dot{W} \\ P \\ \dot{P} \\ Q \\ \dot{Q} \end{bmatrix} = \begin{bmatrix} 0 & 1 & 0 & 0 & 0 & 0 & 0 & 0 & 0 & 0 \\ 0 & 0 & 0 & 0 & 0 & 0 & 0 & 0 & 0 & -W \\ 0 & 0 & 1 & 0 & 0 & 0 & 0 & 0 & 0 & 0 \\ 0 & 0 & 0 & 0 & 1 & 0 & 0 & W & 0 & 0 \\ 0 & 0 & 0 & Q & 0 & 0 & 0 & 0 & 0 & 0 \\ 0 & 0 & 0 & 0 & 0 & 0 & 0 & -V & 0 & 0 \\ 0 & 0 & 0 & 0 & 0 & 0 & 0 & 1 & 0 & 0 \\ 0 & 0 & 0 & 0 & 0 & 0 & 0 & 0 & 0 & \frac{(I_{yy}-I_{zz})}{I_{xx}} \\ 0 & 0 & 0 & 0 & 0 & 0 & 0 & 0 & 0 & 1 \\ 0 & 0 & 0 & 0 & 0 & 0 & 0 & \frac{(I_{zz}-I_{xx})}{I_{yy}} & 0 & 0 \end{bmatrix} \begin{bmatrix} X_E \\ U \\ Y_E \\ V \\ Z_E \\ W \\ \phi \\ P \\ \theta \\ Q \end{bmatrix} + \begin{bmatrix} 0 & 0 & 0 & 0 & 0 \\ \frac{1}{m} & 0 & 0 & 0 & 0 \\ 0 & 0 & 0 & 0 & 0 \\ 0 & \frac{1}{m} & 0 & 0 & 0 \\ 0 & 0 & 0 & 0 & 0 \\ 0 & 0 & 0 & \frac{1}{m} & 0 \\ 0 & 0 & 0 & 0 & 0 \\ 0 & 0 & 0 & \frac{1}{I_{xx}} & 0 \\ 0 & 0 & 0 & 0 & 0 \\ 0 & 0 & 0 & 0 & \frac{1}{I_{yy}} \end{bmatrix} \begin{bmatrix} F_x \\ F_y \\ F_z \\ L \\ M \end{bmatrix} \tag{55}$$

$$\boldsymbol{\dot{x}} = \boldsymbol{A}\boldsymbol{x} + \boldsymbol{B}\boldsymbol{u}$$

$$\begin{bmatrix} y_1 \\ y_2 \\ y_3 \\ y_4 \\ y_5 \end{bmatrix} = \begin{bmatrix} 1 & 0 & 0 & 0 & 0 & 0 & 0 & 0 & 0 & 0 \\ 0 & 0 & 1 & 0 & 0 & 0 & 0 & 0 & 0 & 0 \\ 0 & 0 & 0 & 0 & 1 & 0 & 0 & 0 & 0 & 0 \\ 0 & 0 & 0 & 0 & 0 & 0 & 1 & 0 & 0 & 0 \\ 0 & 0 & 0 & 0 & 0 & 0 & 0 & 0 & 1 & 0 \end{bmatrix} \begin{bmatrix} X_E \\ U \\ Y_E \\ V \\ Z_E \\ W \\ \phi \\ P \\ \theta \\ Q \end{bmatrix} + \begin{bmatrix} 0 & 0 & 0 & 0 & 0 \\ 0 & 0 & 0 & 0 & 0 \\ 0 & 0 & 0 & 0 & 0 \\ 0 & 0 & 0 & 0 & 0 \\ 0 & 0 & 0 & 0 & 0 \end{bmatrix} \begin{bmatrix} F_x \\ F_y \\ F_z \\ L \\ M \end{bmatrix} \tag{56}$$

$$\boldsymbol{y} = \boldsymbol{C}\boldsymbol{x} + \boldsymbol{D}\boldsymbol{u}$$

In this research, the control focus is on the aircraft's attitude motion, which includes controlling roll and pitch rotation motion. Therefore, Eq. (55) and (56) are reduced to a new state space from Eq. (57) to (58).

$$\begin{bmatrix} P \\ \dot{P} \\ Q \\ \dot{Q} \end{bmatrix} = \begin{bmatrix} 0 & 1 & 0 & 0 \\ 0 & 0 & 0 & \frac{(I_{yy}-I_{zz})}{I_{xx}} \\ 0 & 0 & 0 & 1 \\ 0 & \frac{(I_{zz}-I_{xx})}{I_{yy}} & 0 & 0 \end{bmatrix} \begin{bmatrix} \phi \\ P \\ \theta \\ Q \end{bmatrix} + \begin{bmatrix} 0 & 0 \\ \frac{1}{I_{xx}} & 0 \\ 0 & 0 \\ 0 & \frac{1}{I_{yy}} \end{bmatrix} \begin{bmatrix} L \\ M \end{bmatrix} \tag{57}$$

$$\boldsymbol{\dot{x}} = \boldsymbol{A}\boldsymbol{x} + \boldsymbol{B}\boldsymbol{u}$$

https://doi.org/10.31436/iiumej.v25i2.3119

$$\begin{bmatrix} y_4 \\ y_5 \end{bmatrix} = \begin{bmatrix} 1 & 0 & 0 & 0 \\ 0 & 0 & 1 & 0 \end{bmatrix} \begin{bmatrix} \phi \\ P \\ \theta \\ Q \end{bmatrix} + \begin{bmatrix} 0 & 0 \\ 0 & 0 \end{bmatrix} \begin{bmatrix} L \\ M \end{bmatrix} \quad (58)$$

$$\boldsymbol{y} = \boldsymbol{C} \boldsymbol{x} + \boldsymbol{D} \boldsymbol{u}$$

Then, to handle changes in system behavior toward the LQR, the control system will be assisted by a neural network. The neural network can adjust the K LQR gain value to changes in system dynamics both internally and externally so that the aircraft can provide high-stability flights. Therefore, the design of the anatomical structure of the aircraft control system is shown in the block diagram in Figure 3.

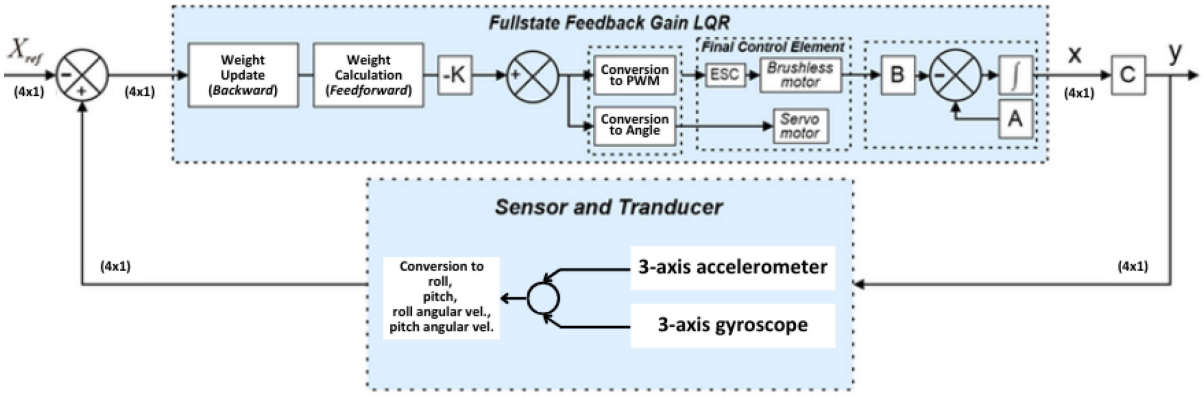

Figure 3. Control system design of flying wing UAV

In this system, there are system input values, which can be predetermined or variable values, which can be changed through control with a remote controller. The reference input value will be compared with the sensor reading value. The difference between the sensor reading and the set point value is called the error value. This error value is used as a reference for the controller to control the system so that it matches the desired reference value or set point. The output from the final control element usually also contains interference from outside the system. The output of the final control element, which is different from the input disturbance, will be considered a running system process. The system will analyze the output of the process by reading through the sensor used. The analysis is done to improve system control if the control is not as desired [27].

The control system on the UAV flying wing for attitude control uses full-state feedback control with four states from the sensor input. The input results are then entered into the full-state feedback system by multiplying the input results by the constant K in a matrix (4x1). The K constant value in this system was previously processed using an artificial neural network system. This artificial neural network system will change the K value tuned using the LQR system with constant Q and R values on each axis and then operate with Riccati calculations. Entering this artificial neural network is the same as entering the system on a flying wing UAV. The u value is the process input calculated by multiplying the feedback gain with the system's state to be controlled. This control input signal will then be used to control the speed of each rotor. Each rotor is a final control element in the UAV flying wing system.

The neural network architecture that works on the LQR control system is shown in Figure 4 [28],

https://doi.org/10.31436/iiumej.v25i2.3119

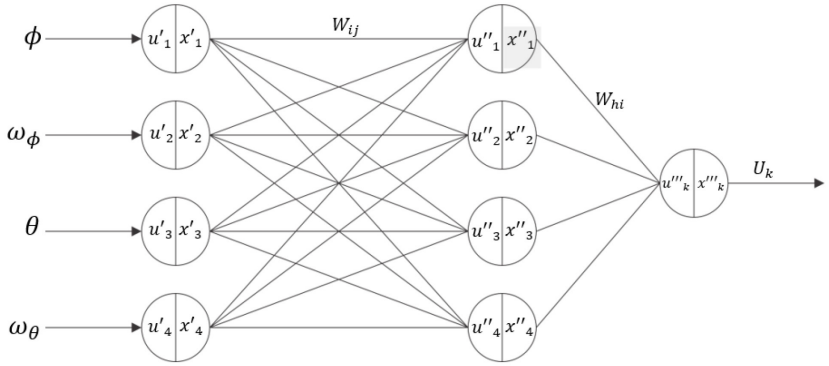

Figure 4. Neural network architecture

3.1 Input Layer

The input layer is input to the neural network system. Enter this system using four entries. Entering the neural network using input as in Figure 4 is intended so that the input to the neural network is the same as the input in the UAV flying wing control system itself.

3.2 Hidden Layer

In the hidden layer of the artificial neural network, six nodes are used. The input from the hidden layer in the artificial neural network is the sum of the multiplication of the Wij weights with the activation value of the node. Where i is the sequence of input nodes, and j is the sequence of hidden nodes.

3.3 Output Layer

In the output layer, there is one node that obtains a value from the sum of the multiplication of weights $Wh1$ and the output from the hidden node x 2. Activation at each node in the three layers uses the sigmoid activation function. The activation function aims to keep the values of each node in each layer from being excessive and still correlated with each other at each layer. This neural network system uses initial weight initialization Wij with Eq. (59).

$$W_{ij} = \begin{bmatrix} 1 & 1 & 0 & 0 & \cdots & 0 & 0 & 0 & 0 \\ 0 & 0 & 1 & 1 & & 0 & 0 & 0 & 0 \\ 0 & 0 & 0 & 0 & & 1 & 1 & 0 & 0 \\ 0 & 0 & 0 & 0 & & 0 & 0 & 1 & 1 \end{bmatrix} \quad (59)$$

Meanwhile, the neural network weight values from the hidden layer to the output layer use the initial value of the constant K resulting from tuning using the LQR method. Form the weight Whi using Eq. (60).

$$W_{hi} = [\mathrm{K}_{11}\ \mathrm{K}_{21}\ \mathrm{K}_{12}\ \mathrm{K}_{22}\ \mathrm{K}_{13}\ \mathrm{K}_{23}\ \mathrm{K}_{14}\ \mathrm{K}_{24}] \quad (60)$$

The weight value Whi in this system is a representation of the feedback constant value used in the flying wing UAV control system. The relationship between artificial neural networks and full-state feedback control here is in tuning the previous K value, which has been determined by the LQR method. The K value is entered as the initial weight value in the weight Whi.

https://doi.org/10.31436/iiumej.v25i2.3119

3.4 Back-propagation Algorithm

The artificial neural network system in this control design uses system error values originating from system output in real-time. The system response is analyzed by calculating the system output error value in the form of four states, which are represented by certain values. The error value in this system is in the form of a sensor reading value in the system, which is then compared with the system reference state value. The main objective of the artificial neural network in this system is to minimize the mean value of the system error squared (J). This system uses the error function Eq. (41). The value is the system output in the form of sensor readings. The value $\boldsymbol{xref}$ is a system reference value in the form of a system input or desire value. In the research $\boldsymbol{xref}$ the signal input of controllability state roll and pitch rotation is set at zero value. The value $y(n)$ is the value of the system output at each system state. The difference between these two values is a system error value. The n value is the number of states observed in this system, namely, four system states.

$$j = E_p = \sum_n \frac{1}{2} \left(y_{(n)} - X_{ref(n)}\right)^2 \tag{61}$$

The learning rate function with a weight change function of 0.01 is used. The weight value Whi will always change depending on the input to the artificial neural network system [29]. These weight values are then used to determine the output in the full-state feedback control system.

Determines the weight value from the hidden layer to the output layer.

To find the weight value from the node Whi hidden layer to the output layer, use Eq. (62) to (67).

$$w_{h1}(k+1) = w_{h1}(k) - \eta \frac{\partial j}{\partial w_{h1}} \tag{62}$$

where n is the learning rate with a value of 0.01. The delta J value is obtained by Eq. (62).

$$\frac{\partial j}{\partial w_{h1}} = \frac{\partial j}{\partial y} . \frac{\partial y}{\partial u} . \frac{\partial u}{\partial w_{h1}} \tag{63}$$

Where y is the response output from the UAV flying wing control system. The u_k Value is the output of the results of the artificial neural network calculation. The value Whi is the weight value from the hidden layer to the output layer of the artificial neural network. From Eq. (63), Eq. (64) is translated to Eq. (66) [30].

$$\frac{\partial j}{\partial y} = x_h^2(k) \tag{64}$$

$$\frac{\partial y}{\partial u} = \frac{\partial y}{\partial t} / \frac{\partial u}{\partial t} = \frac{\dot{y}}{\dot{u}} \approx \frac{\Delta y}{\Delta u} = \frac{y(k)-y(k-1)}{u(k)-u(k-1)} \tag{65}$$

$$\frac{\partial u}{\partial h_1} = \sum_n \frac{1}{2} \left(y_{(n)} - X_{ref(n)}\right)^2 \tag{66}$$

The value $xh1$ is the activation value of the hidden layer, and the y value is the output of the full-state feedback control system. Translating Eq. (62) to Eq. (66) yields Eq. (67), which can be used to obtain the new weight value $xh1$.

$$\frac{\partial j}{\partial w_{h1}} = x_h^2(k) . \frac{y(k)-y(k-1)}{u(k)-u(k-1)} . \sum_n \frac{1}{2} (y_{(n)} - X_{ref(n)})^2 \tag{67}$$

Determine the weight value from the insert layer to the hidden layer. To find the weight value from node i of the insert layer to node j of the hidden layer using Eq. (68).

$$w_{ij}(k+1) = w_{ij}(k) - \eta \frac{\partial j}{\partial w_{ij}} \tag{68}$$

where n is the learning rate with a value of 0.01. The value of delta J is obtained by Eq. (69).

$$\frac{\partial j}{\partial w_{ij}} = \frac{\partial j}{\partial y} . \frac{\partial y}{\partial u} . \frac{\partial u}{\partial w_{ij}} \tag{69}$$

The value Wij is the weight value from the hidden layer to the output layer of the artificial neural network. From Eq. (49), it is explained from Eq. (63) to Eq. (65). The x value is the value resulting from the activation of the hidden layer, so we can obtain Eq. (70) to get the new weight value Wij.

$$\frac{\partial j}{\partial w_{ij}} = W_{h1} X_i^1(k) . \frac{y(k)-y(k-1)}{u(k)-u(k-1)} \sum_n \frac{1}{2} \left(y_{(n)} - X_{ref(n)}\right)^2 \tag{70}$$

4. STRUCTURE AND PARAMETERS OF UAV FLYING WING

The aircraft used in this study have the dimensions shown in Table 1, while Figure 5 illustrates the size and position of the actuator.

Table 1. UAV flying wing dimension

Items	Dimension
Wingspan	1100 mm
Fuselage	500 mm
Winglet	200 mm
Motor Diameter	35 mm
Weight	1300 gram

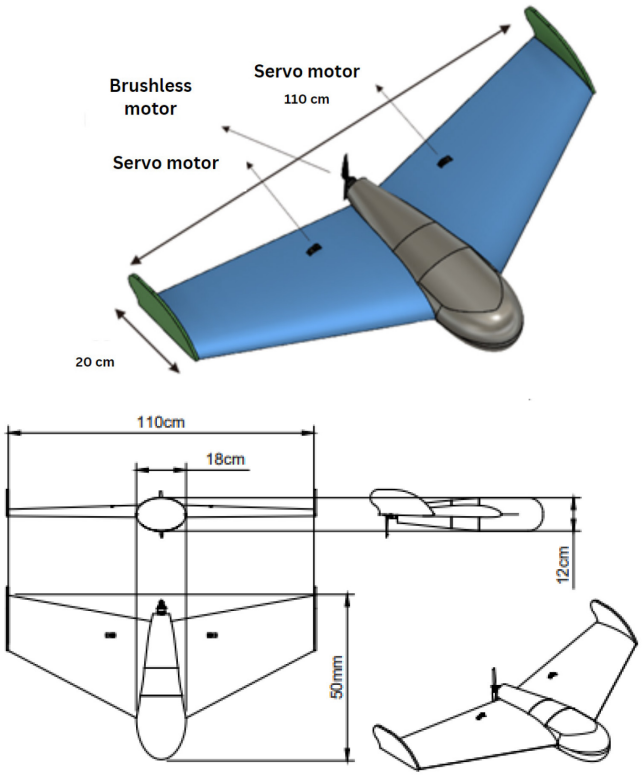

Figure 5. UAV flying wing structure

https://doi.org/10.31436/iiumej.v25i2.3119

The aircraft has dimensions of around 110 cm for the wing length, and the aircraft's flying weight is around 1.3 kg. The body of the aircraft is made from carbon fiber using a molding method to produce a body that is precise, strong, and light. The wings of the aircraft are made from high-density hard foam and coated with fiberglass. The airfoil design on the wing is chosen for the flat bottom type because wings with a flat bottom tend to provide better longitudinal stability. The center of pressure on a flat profile is closer to the balance point. This profile tends to have higher pitch stability, that is, the ability to keep the angle of attack relatively stable. So it can produce low flight speeds.

In proving the control system design, the important thing that is needed is the calculation parameters of the system on the aircraft. One important parameter is the inertia calculation for each axis. The inertia calculations used in this research are the x, y, and z-axis inertia, where each inertia is calculated according to the data in Table 2.

Table 2. Inertia parameters

Items	Length (m)	Width (m)	Height (m)	Mass (kg)	Shape
Center box (I_{KT})	9.18	0.44	0.08	1.182	briquette
Right-wing Part 1 (I_{SKN1})	0.115	0.27	0.03	0.0725	briquette
Right-wing part 2 (I_{SKN2})	0.115	0.2365	0.03	0.0675	briquette
Right-wing Part 3 (I_{SKN3})	0.115	0.2018	0.03	0.0625	briquette
Right-wing Part 4 (I_{SKN4})	0.115	0.1685	0.03	0.0675	briquette
Left-wing Part 1 (I_{SKR1})	0.115	0.27	0.03	0.0725	briquette
Left-wing part 2 (I_{SKR2})	0.115	0.2365	0.03	0.0675	briquette
Left-wing part 3 (I_{SKR3})	0.115	0.2018	0.03	0.0625	briquette
Left-wing part 4 (I_{SKR4})	0.115	0.1685	0.03	0.0675	briquette

x-axes inertia calculation (I_{xx})

$$I_{xx} = (I_{KTx}) + (I_{SKR1x}) + (I_{SKR2x}) + (I_{SKR3x}) + (I_{SKR4x}) + (I_{SKN1X}) + (I_{SKN2X}) + (I_{SKN3X}) + (I_{SKN4X})$$

$$I_{xx} = 1{,}97\ x\ 10^{-2} + 4{,}46\ x\ 10^{-4} + 3{,}19\ x\ 10^{-4} + 2{,}17\ x\ 10^{-4} + 1{,}40\ x\ 10^{-4} + +4{,}46\ x\ 10^{-4} + 3{,}19\ x\ 10^{-4} + 2{,}17\ x\ 10^{-4} + 1{,}40\ x\ 10^{-4}$$

$$\boldsymbol{I_{xx} = 2{,}194\ x\ 10^{-2}\ \text{Kg}.m^2}$$

y-axes inertia calculation (I_{yy})

$$I_{yy} = (I_{KTy}) + (I_{SKR1y}) + (I_{SKR2y}) + (I_{SKR3y}) + (I_{SKR4y}) + (I_{SKN1y}) + (I_{SKN2y}) + (I_{SKN3y}) + (I_{SKN4y})$$

$$I_{yy} = 3{,}82\ x\ 10^{-3} + 8{,}53\ x\ 10^{-5} + 7{,}94\ x\ 10^{-5} + 7{,}36\ x\ 10^{-5} + 6{,}77\ x\ 10^{-5} + 8{,}53\ x\ 10^{-5} + 7{,}94\ x\ 10^{-5} + 7{,}36\ x\ 10^{-5} + 6{,}77\ x\ 10^{-5}$$

$$\boldsymbol{I_{yy} = 4{,}434\ x\ 10^{-3}\ \text{Kg}.m^2}$$

z-axes inertia calculation (I_{zz})

$$I_{zz} = (I_{KTz}) + (I_{SKR1z}) + (I_{SKR2z}) + (I_{SKR3z}) + (I_{SKR4z}) + (I_{SKN1z}) + (I_{SKN2z}) + (I_{SKN3z}) + (I_{SKN4z})$$

$$I_{zz} = 2{,}23\ x\ 10^{-2} + 5{,}20\ x\ 10^{-4} + 3{,}89\ x\ 10^{-4} + 2{,}81\ x\ 10^{-4} + 1{,}99\ x\ 10^{-4} + 5{,}20\ x\ 10^{-4} + 3{,}89\ x\ 10^{-4} + 2{,}81\ x\ 10^{-4} + 1{,}99\ x\ 10^{-4}$$

$$\boldsymbol{I_{zz} = 2{,}50\ x\ 10^{-2}\ \text{Kg}.m^2}$$

https://doi.org/10.31436/iiumej.v25i2.3119

5. RESULT AND DISCUSSIONS

In this research, the implementation of the LQR-NN control system was carried out through simulation using MATLAB. The application is preceded by searching for the K LQR gain value from the best response obtained. The calculation of the feedback gain K value for each state involved is sought by tuning the value of the Q element. From the experiments that have been carried out, the best Q value from the results of roll and pitch anti-rotation motion control is shown in Table 3, where the data shows the best conversion of Q and R values to obtain the most optimal K gain value [31].

Table 3. Conversion metrics **Q** values to gain **K** values

Q	R	Gain K
$\begin{bmatrix} 1.0245 & 0 & 0 & 0 \\ 0 & 0.00049 & 0 & 0 \\ 0 & 0 & 1.033 & 0 \\ 0 & 0 & 0 & 0.004 \end{bmatrix}$	1	$\begin{bmatrix} 1.0124 & 0.2119 & 0 & 0 \\ 0 & 0 & 1.0149 & 0.1140 \end{bmatrix}$

The best K gain value can control the aircraft's attitude, both roll and pitch angles, with the signals shown in Figures 6 and 7. Figure 6 is for roll stability, and Figure 7 is for pitch stability.

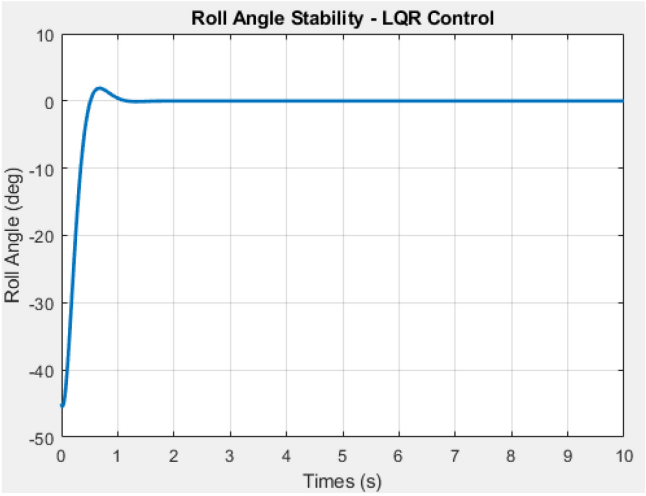

Figure 6. Roll angle stability using LQR

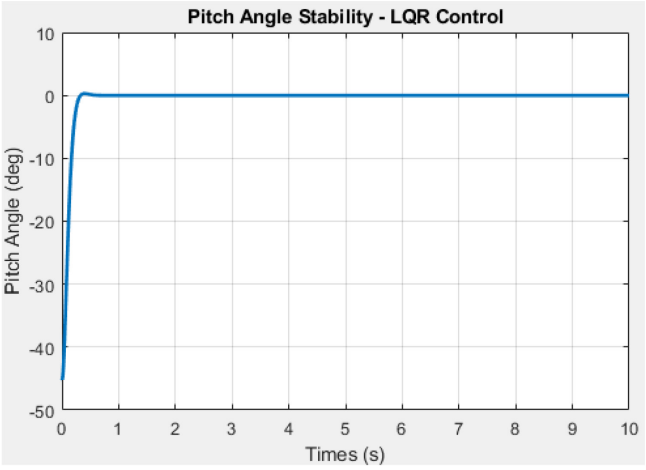

Figure 7. Pitch angle stability using LQR

https://doi.org/10.31436/iiumej.v25i2.3119

The two aircraft flight movements shown in Figures 6 and 7 have stability characteristics, which are explained through the transient response in Table 4.

Table 4. Transient response of roll and pitch stability using LQR control

Components	Roll	Pitch
Rise time	0.4682s	0.2455s
Overshoot	4.217%	0.6311%
Settling time	1.149s	0.7091s
Steady-state error (SSE)	-0.007deg	-0.0001deg

According to Table 5, the pitch angle demonstrates superior stability compared to the roll angle. With a rise time of 0.2227 seconds and a settling time of 0.44 seconds, the pitch response is faster than that of the roll. Additionally, the pitch displays minimal overshoot, measuring at 0.6311% or under 1%. Furthermore, its steady-state error is -0.0001 degrees, smaller than the roll's error of -0.0007 degrees. This discrepancy can be attributed to the aircraft's predominantly wing-based construction, making it susceptible to lateral disturbances such as side interference or slip. Moreover, larger torque occurrences slow down the control system's ability to mitigate disturbances effectively.

Apart from this, the characteristics of the roll and pitch angles show good stability. Tests carried out on the control of both states prove that the LQR control is able to maintain the stability of the roll and pitch torque against the given disturbances. Apart from that, the test shows that the greater the weighting of the Q element, the greater the K gain value will be. The greater the K gain value, the greater the torque on the aircraft system, making the system more responsive compared to a small K gain value. Of the two controlled states, roll and pitch motion will not provide the same character to the system. These two states have complementary roles in stabilizing. It can be seen by giving the K gain value to the angular speed. The greater the K value given to this state, the more the response that occurs in the system will be suppressed or dampened. Angular velocity is the first derivative of the roll orientation angle, which will change if there is a change in angular position relative to the time of change, so the faster the change, the greater the resulting angular velocity [9].

From the best K gain value obtained for each control state, K is used as a reference value in the change value of the artificial neural network. The artificial neural network model has one hidden layer, where the training process is carried out via online learning based on the errors that occur. The error value will be fed back using the backpropagation method, where the weight that changes is the gain value K with a learning rate of 0.01. Setting the learning rate value at this value so as not to force the system to accept signal changes that are too large, which can cause the aircraft to experience turbulence, resulting in a flight stall.

In this initial comparison test, the system will be subjected to a 45-degree deviation as the initial value in the step function. This approach is employed to assess the robust characteristics of the aircraft when stabilizing with relatively large deviations. The outcomes of controlling the stability of the aircraft's attitude using LQR-NN control are depicted in Figures 8 and 9.

https://doi.org/10.31436/iiumej.v25i2.3119

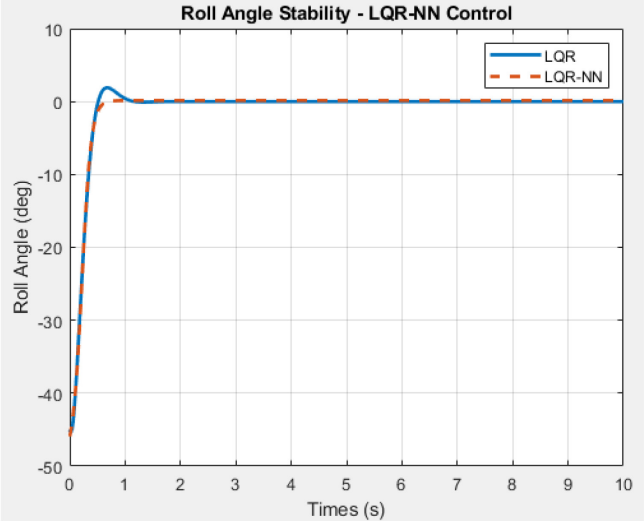

Figure 8. The comparison of roll angle stability between using LQR and LQR-NN

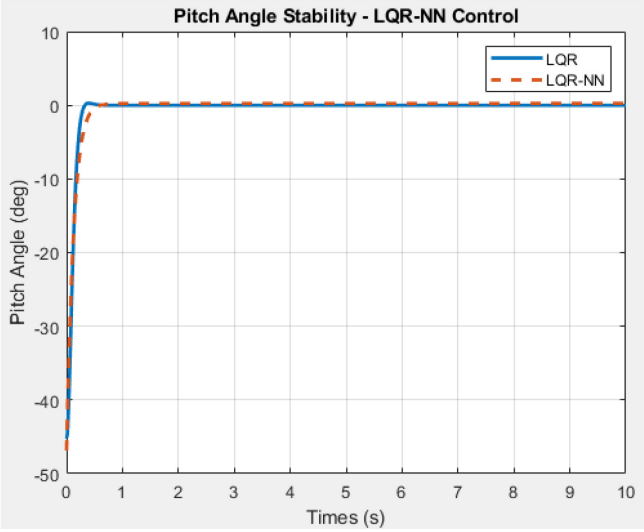

Figure 9. The comparison of pitch angle stability between using LQR and LQR-NN

The results of this control were obtained by setting the net on the neurons to four nets with an epoch of 82. The experiments revealed that setting the epoch value above 82 causes oscillations in the system. In contrast, values below 82 have minimal impact on the neural network, thus ensuring stability across all controlled states without altering their characteristics [32]. LQR-NN control of roll and pitch angles provides the characteristics shown in Table 5.

Table 5. The comparison of the transient response of roll and pitch stability between using LQR and LQR-NN control

Components	LQR		LQR-NN		Minimum Requirements of Aircraft
	Roll	Pitch	Roll	Pitch	
Rise time	0.4682s	0.2455s	0.4682s	0.2309s	< 1s
Overshoot	4.217%	0.6311%	0.298%	0.1224%	< 3%
Settling time	1.149s	0.7091s	1.3819s	0.7091s	< 3s

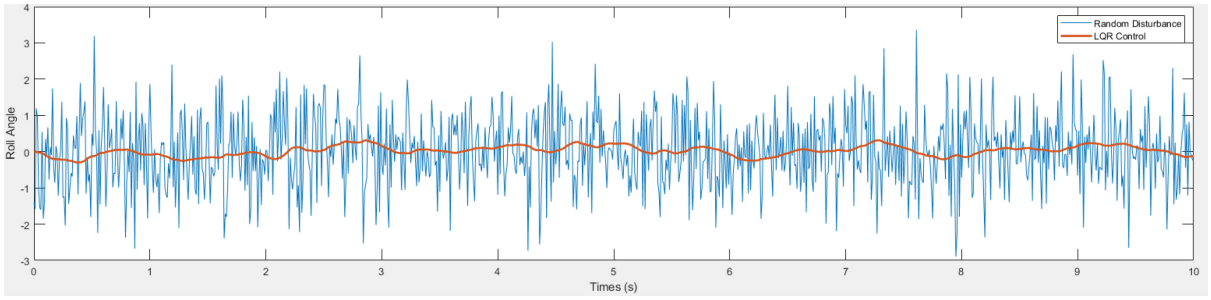

(a)

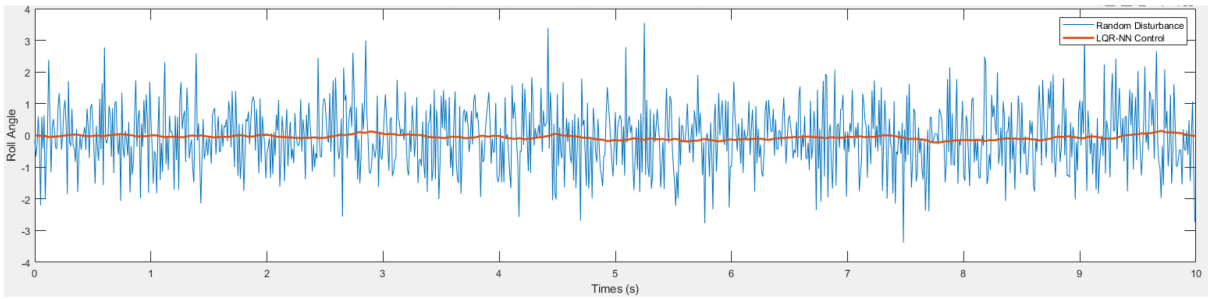

(b)

Figure 10. (a) Roll angle stability control using LQR in handling random disturbances (b) Roll angle stability control using LQR-NN in handling random disturbances

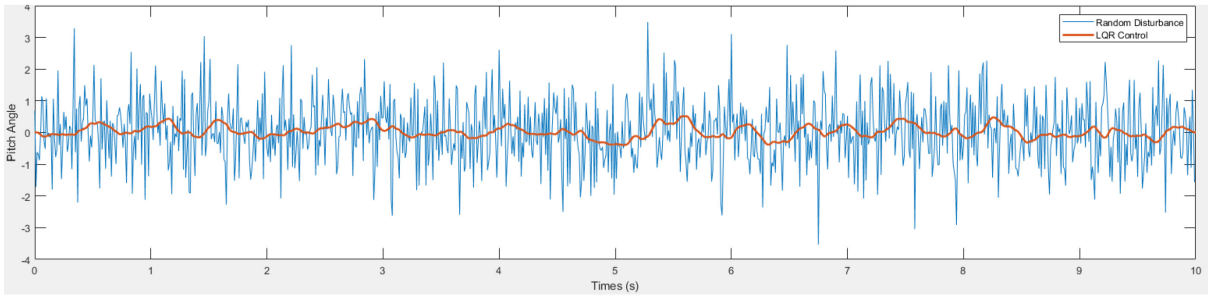

(a)

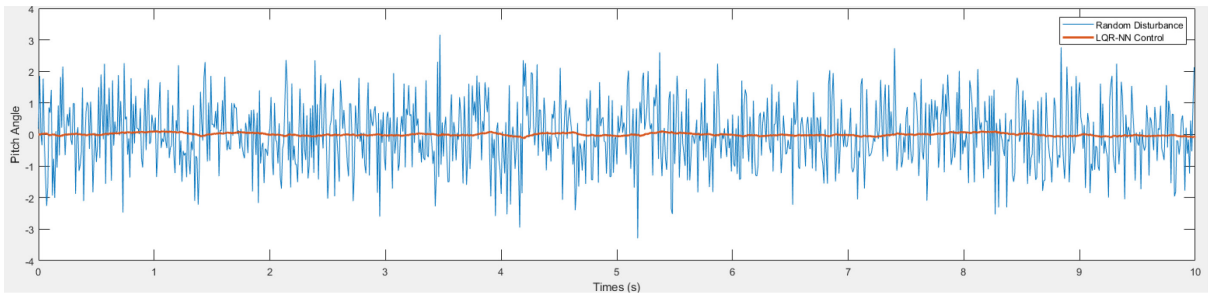

(b)

Figure 11. (a) Roll angle stability control using LQR in handling random disturbances (b) Roll angle stability control using LQR-NN in handling random disturbances

Based on Table 6, roll and pitch flight attitude with LQR-NN control has better equilibrium characteristics than LQR. The LQR-NN control can minimize overshoot during pitch and roll rotational motion to less than 1%, whereas the LQR control only meets the minimum required pitch motion criteria. Significant changes occurred in the overshoot value, which was further reduced by neural network predictions. This is important in control because the greater the

overshoot, the greater the possibility of producing multiple overshoots, which can make the flight unstable and even cause the plane to crash [33].

Furthermore, the management of steady-state error (SSE) by the LQR-NN control system surpasses that of the LQR control system. LQR-NN effectively reduces SSE to a lesser degree. This is evidenced by the graphical simulation results depicted in Figures 10 and 11.

In this observation, the system experienced random disturbances for 10 seconds. The simulation results demonstrate that LQR-NN effectively maintains SSE at 0.074 degrees for roll rotation motion and 0.035 degrees for pitch rotation motion. In contrast, LQR control maintains SSE at 0.113 degrees for roll rotation motion and 0.150 degrees for pitch rotation motion during flight. LQR-NN exhibits greater adaptability to the occurring disturbances. LQR-NN has been deemed to meet the criteria for a highly proficient control system because it satisfies all the minimum specification requirements for system response stability, particularly in the flight attitude of the UAV flying wing aircraft.

6. CONCLUSION

LQR-NN control has been successfully modeled and applied to control the stability of the roll and pitch flight attitude of UAV flying-wing aircraft. The net settings given to the hidden layer neural network are four nets with an epoch of 82. The test results show that roll angle stability has characteristics of a rise time of 0.4682 seconds, settling time of 1.3819 seconds, overshoot of 0.298%, and SSE of 0.133 degrees, while pitch angle stability has a rise time of 0.2309 seconds, settling time of 0.7091 seconds, overshoot of 0.1224% and SSE of 0.0239 degrees. LQR-NN can reduce overshoot that occurs in the LQR controller so that it can minimize oscillations that will occur. Additionally, LQR-NN effectively mitigates the steady-state error (SSE), reducing it to 0.074 degrees for roll rotation motion and 0.035 degrees for pitch rotation motion.

REFERENCES

[1] Mátyás P, Nagy M. (2019). Brief history of uav development. Repüléstudományi Közlemények, 31(1): 155-6. https://doi.org/10.32560/rk.2019.1.13

[2] Andres AM, Yilei H, Yuhan J. (2023). A review of unmanned aerial vehicle applications in construction management: 2016–2021. Standards. 3(2): 95–109. https://doi.org/10.3390/standards3020009

[3] Tri KP, Oktaf AD, Tri S. (2020). Model of linear quadratic regulator (lqr) control system in waypoint flight mission of flying wing uav. Journal of Telecommunication, Electronic and Computer Engineering (JTEC), 12(4): 43–49. https://jtec.utem.edu.my/jtec/article/view/5696

[4] Stavros K, Chris B, Pavlos K, Pericles P, Kyros Y. (2023). Parametric investigation of canards on a flying wing uav using the taguchi method. Aerospace, 10(3): 264. https://doi.org/10.3390/aerospace10030264

[5] Seyhun D. (2023). Aerodynamic performance comparison of airfoils in flying wing uav. International Journal of Innovative Engineering Applications, 7(1): 123–127. https://doi.org/10.46460/ijiea.1169652

[6] Panjani D, Indira P, Chandu A. (2022). Design of folded wing mechanism for unmanned aerial vehicle (uav). Materials Today: Proceedings, 62: 4117–4125. https://doi.org/10.1016/j.matpr.2022.04.660

[7] Yankui W, Xiangxi T, Tao L. (2020). Lateral stability and control of a flying wing configuration aircraft. Journal of Physics: Conference Series, 1509(1): 012022. https://doi.org/10.1088/1742-6596/1509/1/012022

[8] Jose DH, Camilo E, Juan PA, Gustavo S, Juliana AN, Jorge IG. (2023). Two-way coupled aero-structural optimization of stable flying wings, Aerospace. 10(4): 346. https://doi.org/10.3390/aerospace10040346

[9] Oktaf AD, Andi D, Tri KP. (2017). Model of linear quadratic regulator (lqr) control method in hovering state of quadrotor. Journal of Telecommunication, Electronic and Computer Engineering (JTEC), 9(3): 135–143. https://jtec.utem.edu.my/jtec/article/view/1589

[10] Oktaf AD, Faisal FR. (2022). Peningkatan kestabilan quadrotor menggunakan kendali linear quadratic regulator dengan kompensasi integrator dalam mempertahankan posisi. Buletin Ilmiah Sarjana Teknik Elektro. 4(2): 62–75. https://doi.org/10.12928/biste.v4i2.6808

[11] Riccardo D, Piero T, Salvatore FG, Alessandro M. (2021). Recent advances in unmanned aerial vehicle forest remote sensing - a systematic review, part i: a general framework. Forests. 12(3): 327. https://doi.org/10.3390/f12030327

[12] Jingjing B, Afshin M, Maryam F, Mehran M. (2019). Lqr through the lens of first order methods: discrete-time case. https://doi.org/10.48550/ARXIV.1907.08921

[13] Aisha SE, Seref NE. (2022). Robust lqr and lqr-pi control strategies based on adaptive weighting matrix selection for a uav position and attitude tracking control. Alexandria Engineering Journal, 61(8): 6275–6292. https://doi.org/10.1016/j.aej.2021.11.057

[14] Jinsong Z, Yan L, Lin L. (2023). LQR-based adaptive optimal control for aircraft engine. Proceedings of 2023 Chinese Intelligent Systems Conference. CISC 2023. Lecture Notes in Electrical Engineering, vol 1090. Springer, Singapore. https://doi.org/10.1007/978-981-99-6882-4_28

[15] Faisal FR, Tri KP. (2019). Penalaan mandiri full state feedback lqr dengan jst tiruan pada kendali quadrotor. Indonesian Journal of Electronics and Instrumentation Systems (IJEIS). 9(1): 21-32. https://doi.org/10.22146/ijeis.37212

[16] Chenxi S, Tao L, Kui Y. (2013). Balance control of two-wheeled self-balancing robot based on Linear Quadratic Regulator and Neural Network. 2013 Fourth Int. Conf. Intell. Control Inf. Process. 1: 862–867. https://doi.org/10.1109/ICICIP.2013.6568193

[17] Huynh VN, Dinh PN, Nguyen TMN, Nguyen TD, Nguyen PL, Phung ST, Le THL, Dang XB. (2021). A lqr-based neural-network controller for fast stabilizing rotary inverted pendulum. 2021 International Conference on System Science and Engineering (ICSSE), 19–22. https://doi.org/10.1109/ICSSE52999.2021.9537940

[18] John BH. (2007). Modelling Simulation and Control of Fixed-wing UAV: CyberSwan. Institutt for teknisk kybernetikk.

[19] Tri KP, Abdul MF. (2021). Modeling and Simulation of The UX-6 Fixed-Wing Unmanned Aerial Vehicle. J Control Autom Electr Syst 32, 1344–1355. https://doi.org/10.1007/s40313-021-00754-5

[20] Burak E. (2019). Fault tolerant flight control applications for a fixed wing uav using linear and nonlinear approaches. https://doi.org/10.13140/RG.2.2.25180.03205

[21] Jie C, Jianxin L. (2021). Mathematical modeling and fault tolerant control of uav with wing layout. Journal of Physics: Conference Series, 1846(1): 012045. https://doi.org/10.1088/1742-6596/1846/1/012045

[22] Ruijie S, Zhou Z, Xiaoping Z. (2022). Stability control of a fixed full-wing layout uav under manipulation constraints. Aerospace Science and Technology, 120: 107263. https://doi.org/10.1016/j.ast.2021.107263

[23] Aman S, Gabriel FL, Jan S. (2023). Identifying aerodynamics of small fixed-wing drones using inertial measurements for model-based navigation. NAVIGATION: Journal of the Institute of Navigation, 70(4): navi.611. https://doi.org/10.33012/navi.611

[24] Yuqiong S, Song W, Anastasiia K, Yujing H. (2019). Attitude control of flying wing uav based on advanced adrc. IOP Conference Series: Materials Science and Engineering, 677(5): 052075. https://doi.org/10.1088/1757-899X/677/5/052075

[25] Shi Q, Cui H, Li F, Liu Y, Ju W, Sun Y. (2017). A hybrid dynamic demand control strategy for power system frequency regulation. CSEE J Power Energy Syst, 3(2):176–185. https://doi.org/10.17775/CSEEJPES.2017.0022

[26] Jianglin L, Dezong Z. (2023). Finding the lqr weights to ensure the associated riccati equations admit a common solution. IEEE Transactions on Automatic Control, 68(10): 6393–6400. https://doi.org/10.1109/TAC.2023.3234237

[27] Gembong ES, Wijaya K, Amroy CLG. (2019). Linear quadratic regulator controller (lqr) for ar. drone's safe landing. 2019 International Conference on Sustainable Information Engineering and Technology (SIET), 228–233. https://doi.org/10.1109/SIET48054.2019.8986078

[28] Mahmud S. (2021). Modelling and simulation of small scale fixedwing autonomous aerial vehicles. PhD Thesis. Sheffield Hallan University, Business, Technology and Engineering.

[29] Faisal FR, Tri KP. (2019). Penalaan mandiri full state feedback dengan lqr dan jst pada kendali quadrotor. IJEIS (Indonesian Journal of Electronics and Instrumentation Systems), 9(1): 21. https://doi.org/10.22146/ijeis.37212

[30] Bailun J, Boyang L, Weifeng Z, Li-Yu L, Chih-Keng C, Chih-Yung C. (2022). Neural network based model predictive control for a quadrotor uav. Aerospace, 9(8): 460. https://doi.org/10.3390/aerospace9080460

[31] Yunlong G, Guixin Z, Tong Z. (2022). Based on backpropagation neural network and adaptive linear active disturbance rejection control for attitude of a quadrotor carrying a load. Applied Sciences, 12(24): 12698. https://doi.org/10.3390/app122412698

[32] Aris T, Suroto M, Munadi M, Joga DS. (2023). Application of driving behavior control system using artificial neural network to improve driving comfort by adjusting air-to-fuel Ratio. IIUM Engineering Journal, 24(2): 337–353. https://doi.org/10.31436/iiumej.v24i2.2781

[33] Oktaf AD, Tri KP, Aris N, Yasir MM. (2022). Enhancement of stability on autonomous waypoint mission of quadrotor using lqr integrator control. IIUM Engineering Journal, 23(1): 129–158. https://doi.org/10.31436/iiumej.v23i1.1803